Proceedings of the Seventh International ASME Conference on Nanochannels, Microchannels and Minichannels
ICNMM2009
June 22-24, 2009, Pohang, South Korea

ICNMM2009-82180

DRAFT: STUDY OF GAS FLOW IN MICRONOZZLES USING AN UNSTRUCTURED DSMC SOLVER

Ehsan Roohi
Email: roohi@ae.sharif.edu

Masoud Darbandi
Email: darbandi@sharif.edu

Vahid Mirjalili
Email: v.mirjalili@ae.sharif.edu

Department of Aerospace Engineering, Sharif University of Technology,
P.O. Box 11365-8639, Tehran, Iran.

ABSTRACT

The current research uses an unstructured direct simulation Monte Carlo (DSMC) solver to numerically investigate supersonic and subsonic flow behavior in micro convergent–divergent nozzles over a wide range of rarefaction regime. The unstructured DSMC solver has been optimized via using uniform distribution of particles, suitable subcell geometry, and advanced molecular tracking algorithm. The effects of back pressure, gas/surface interactions (diffuse/specular reflections), and Knudsen number, on the micronozzle flow field were studied. High viscous force manifesting in boundary layers prevents supersonic flow formation at the divergent section of nozzles as soon as the Knudsen number increases above a moderate level. In order to accurately simulate subsonic flow at the nozzle outlet, it is necessary to add a buffer zone to the end of nozzle. If we apply the back pressure at the outlet, boundary layer separation is observed and a region of backward flow appears inside the boundary layer while the core region of inviscid flow experiences multiple shock-expansion waves. We observed that the wall boundary layer prevents formation of normal shocks. Instead, Mach cores appear at the nozzle center followed by bow shocks and expansion region.

1. INTRODUCTION

Interest in Micro/Nano-Electro-Mechanical Systems (MEMS-NEMS) has shown enormous growth for the past few years. This has led to the development of an increasing number of extremely small devices. As the hydrodynamic diameter of a flow conduit decreases to the length comparable with the mean-free-path of the particles moving inside the device, the continuum flow hypothesis in the Navier-Stokes (NS) equations deteriorates. In other words, the gas can no longer be considered in thermodynamic equilibrium and a variety of rarefaction effects take place. The degree of rarefaction for gas is usually expressed by Knudsen number, which is the ratio of gas mean free path to the conduit height, i.e., $Kn=\lambda/H$. Different non-equilibrium regimes, i.e., slip ($0.01<Kn<0.1$), transition ($0.1<Kn<10$), and free molecular ($Kn>10$), can be observed in micro-nano scale geometries.

One of the basic components of micro/nano systems is the convergent-divergent nozzle. Micro/nano nozzle flow usually passes trough different rarefaction regime, i.e., it experiences continuum and slip regime at the convergent section while transition and free molecular regime may occur at the divergent section and nozzle exhaust. In order to simulate fluid flow in micro-nozzles in wide ranges of rarefaction regime, kinetic approaches such as direct simulation Monte Carlo (DSMC) [1] have been applied. DSMC has been widely used to predict the flow field inside micro-scale devices such as microchannels [2-5] and micronozzles.

Alexeenko et al. [6] performed DSMC and continuum simulations for the axisymmetric and three dimensional micronozzles. They observed that viscous effects dominate the gas expansion and thrust losses occur due to significant wall shear stress. They investigated the effect of the tangential momentum accommodation coefficient on the flow and showed that the flow weakly depends on it when this coefficient increases from 0.8 to 1. Louisos and Hitt [7] used the NS equations and studied the geometrical effects on the micronozzle performance. They reported a remarkable reduction in thrust as the divergence half-angle of 2D micronozzles increased above 30°. They reported that the subsonic boundary layer restricts the flow and reduces the

effective exit area. In a further attempt, Alexeenko et al. [8] used a coupled thermal-fluid analysis (finite element-DSMC) to study the performance of high temperature MEMS-based nozzles. They obtained the temporal variation of the nozzle temperature and gas flow fields. In addition, the operational time limits for thermally insulated and convectively cooled nozzles were reported. Liu et al [9] used DSMC and NS equation with slip boundary conditions to simulate nozzle flows. They studied the effects of inlet pressures, Reynolds number and micronozzle geometry. They reported that continuum-based results show obvious deviations from the DSMC results once Kn exceeds 0.045. Xie [10] simulated low Knudsen number micronozzle flows via using DSMC and NS equations. He examined the dependence of mass flux on the pressure difference. He also reported the occurrence of multiple expansion-compression waves in the nozzle's divergent section. Titove and Levin [11] proposed a collision-limiter method, i.e., equilibrium direct simulation Monte Carlo (eDSMC), to extend the DSMC technique to high pressure small-scale nozzle and channel flows. The eDSMC calculations demonstrated the nozzle compression waves and agreed well with the higher order Eulerian solutions. Xu and Zhao [12] used the NS equations with the slip wall boundary conditions to simulate nozzle flow subject to back pressure. They studied shock structures at low Knudsen number. They find that the viscous effect is the key parameter to form the shock wave structure in the micronozzles flows. Louisos et al. [13] reviewed the key findings obtained from computational studies, either continuum or kinetic-based, of supersonic micronozzle. They reported that the combination of viscous, thermal and rarefaction effects on the microscale greatly impact the flow behavior in supersonic micronozzles. Different aspects of rarefaction effects on nozzle performance have been described. They reported that thermal non-equilibrium, i.e., the delay in the rotational and vibrational energy relaxation, would result in performance loss for micronozzles at low Reynolds numbers.

The main objective of the current study is to provide a deeper understanding of convergent-divergent micronozzle flows. We investigate the effects of back pressure, Knudsen number, and gas-surface interaction on the micronozzle behavior. We discuss the correct position where back pressure should be applied. We use DSMC method to confidently simulate micronozzle flow over a wide range of rarefaction regime. Our basic DSMC solver has already been validated for micro-nano channel flow simulations [4, 5]; however, to simulate nozzle flows, the solver has been suitably extended to unstructured grids and optimized.

2. DSMC SCHEME

2.1 Basic Algorithm

DSMC is a numerical tool to solve the Boltzmann equation based on direct statistical simulation of the molecular processes described by the kinetic theory [1]. It is considered as a particle method in which particle represents a large bulk of real gas molecules. The physics of the gas is modeled through uncoupling of the motion of particles and collisions between them. The implementation of DSMC needs breaking down the computational domain into a collection of grid cells. After fulfilling all molecular movements, the collisions between particles are simulated in each cell independently. In the current study, variable hard sphere (VHS) collision model is used and the collision pair is chosen based on the no time counter method [1].

Main steps of the DSMC method include setting up the initial conditions, moving and indexing the particles, colliding particles, and sampling the particles within cells to determine the thermodynamic properties such as temperature, density, and pressure. Following Wang and Li [3], we used the 1-D characteristic theory to apply inlet/outlet pressure boundary conditions. The velocities of the reflected particles were randomly attributed according to the one-half-range Maxwellian distribution. Reflection from symmetry boundary was considered specular. The details of boundary condition implementation are described in Ref. [4].

2.2 Features of Unstructured Code

2.2.1 Subcells Arrangement

The DSMC cells are further divided into subcells. Possible collision pairs are randomly selected from the same subcell. As shown in Fig. 1, we can divide the triangular mesh into three or four subcells. Three subcells arrangement considers the possibility of collision for particles which have the farthest distance from each others, i.e., particles located near the cell vertices. Therefore, the collisions may not be truly physical. Alternatively, four subcells arrangement results in more accurate solution because it considers the possibility of collision for closer particles. Our simulation show that computational time increases up to 25% if we use three subcells arrangement for the same number of grids.

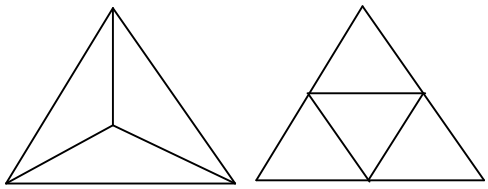

Figure 1. Subcells in triangular mesh; three subcells (left), four subcells (right).

2.2.2 Initial Particle distribution

In DSMC, initial distribution of particles is performed in a random manner. For an arbitrary triangular mesh, we use two different approaches to distribute particles. In the first one, we determine the particle axial position (X) as

$$X = \min(x_1, x_2, x_3) + l \times \max\left(|x_2 - x_1|, |x_3 - x_2|, |x_1 - x_3|\right) \qquad (1)$$

where x_1, x_2, x_3 are the x-coordinate of cell vertices and l is random number. Next, we find the intersections (y_{is1}, y_{is2}) of a vertical line which crosses two sides of triangle. Y position of particle is determined as

$$Y = \min(y_{is1}, y_{is2}) + m \times |y_{is2} - y_{is1}| \qquad (2)$$

where m is another random number. Our experience show that this approach leads to non-uniform distribution and particles will be concentrated near one vertex of the cell, see Fig. 2(a). This results in longer computational time to get converged results. The second approach uses the alternative formulas

$$\begin{aligned} X &= l \times x_1 + m \times x_2 + (1 - l - m) \times x_3 \\ Y &= l \times y_1 + m \times y_2 + (1 - l - m) \times y_3 \end{aligned} \qquad (3)$$

The summation of two random numbers (l, m) must be lower than 1. As shown in Fig. 2-(b), this formula gives more uniform distribution.

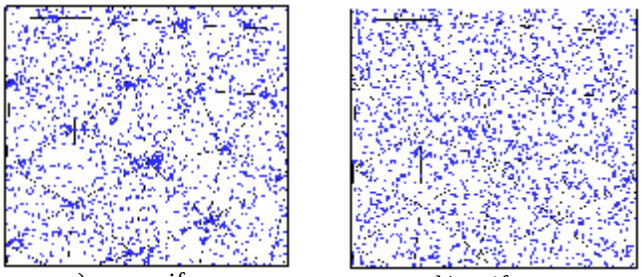

a) non-uniform b) uniform

Figure 2. Initial distribution of particles

2.2.3 Particle Tracking Algorithm

It is straightforward to find the new potion of particles in structured cells because there are simple algebraic relations between particle position and cell geometry. However; a time consuming direct search of meshes may be required to determine the new position of particles in unstructured meshes. One of the basic "direct search" algorithms is refereed to Zhou and Leschziner, i.e., ZL algorithm [13]. The ZL algorithm is simple and needs a little computational time but may search in great number of cells. It benefits from the "point to left" (P2L) idea. P2L states that if a particle is located in the left side of all faces of the cell, i.e., if the cross product of the triangle edge and the connecting edge between particle position and the first vertex of the edge is positive, the particle is located inside the cell. ZL algorithm must be performed for different layers of neighboring cells, therefore; it may be quit time consuming.

The alternative approaches are usually based on "particle tracking". Chen and Pereira [15] suggested a tracking algorithm, i.e., CP algorithm, inside cells located between initial (P_i) and final (P_f) positions of particles. CP algorithm starts with P2L cross product for all edges of the initial cell. If P2L indicates that particle has moved from that cell, the edges with negative P2L are targeted. The intersection of particle path (P_f- P_i) and the above edges are examined. The neighboring cell whose edge involves intersection point is the next target where the P2L product is repeated. We applied CP algorithm in our DSMC solver. Alternative particle tracking algorithms have also been suggested, i.e., see Ref. [16].

3. RESULTS AND DISCUSSION

3.1 Validation & Grid Study

Figure 1 shows the half geometry of the micronozzle and the triangular unstructured grid used to discritize the solution domain. One half of the geometry is simulated due to the symmetry. In all of our studies, we consider nitrogen as the working fluid. The correct implementation of boundary conditions is a critical issue in micro-nano fluid simulations; see Ref. [5, 17-19]. As we will show in next sections, it is necessary to add a buffer zone to the end of nozzle in order to accurately simulate subsonic flow. At the first stage of validating unstructured solver, we compare our nozzle flow solution with our basic structured code.

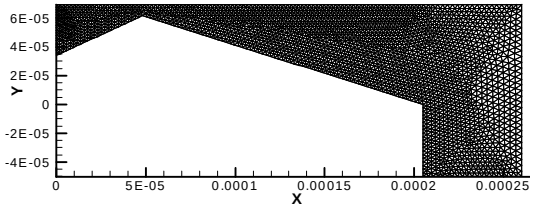

Figure 3. Solution domain in unstructured triangular grid.

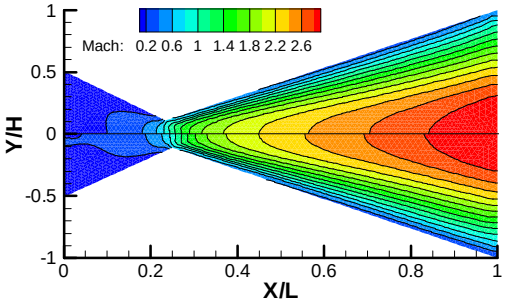

Figure 4. Comparison between structured (top) and unstructured grids solutions (bottom).

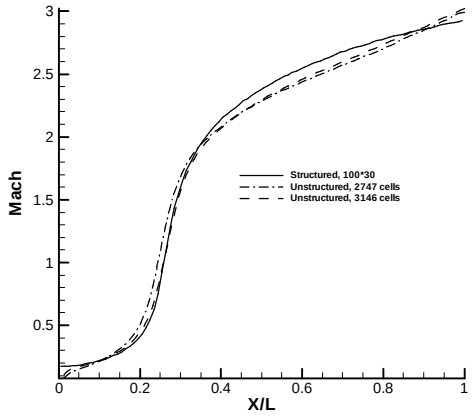

Figure 5. Centerline Mach from different grids

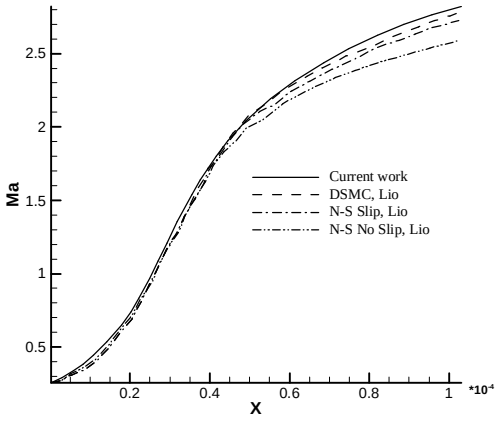

Figure 6. Mach number distribution along the centerline.

Figure 4 shows Mach contours from both structured (100×30) and unstructured grids (2747 cells) for nozzle flow for with $Kn_{in}=4\times10^{-4}$, throat length L_t=15 μm, and P_{in}=0.5 atm. Our experiences proved that low speed subsonic flow at the convergent section of nozzle shows sensitivity to number of cells and particles. Figure 5 shows distribution of centerline

Mach number from structured and two different unstructured grids (2747 cells, 3146 cells). It is observed that there is small difference between the three solutions. Figure 6 compares the distribution of centerline Mach number from current unstructured DSMC solver with the DSMC and NS solutions of Liu et al [9]. Both DSMC solutions are close to each other. Since the Knudsen number is small in the convergent section, DSMC and NS solutions are very close there. But the discrepancy between kinetic and molecular solutions increases as the flow expands and rarefies more in the divergent section.

We study the effects of back pressure, Knudsen number, and gas-surface interaction on the micronozzle behavior. Table 1 provides a summary of the current investigated test cases. Case 1 studies supersonic flow. Cases 2-5 consider the effects of back pressure. We simulate all 5 cases with viscous and inviscid wall boundary conditions. For all the cases, L_t=15 μm, $Kn_{in}=4\times10^{-4}$, and $T_{wall}=T_{in}=300$ K. Two sets of data for $\overline{Kn}_0$ are reported, i.e., one for viscous and another for inviscid walls. Reynolds number, based on the throat height, is only reported for viscous cases.

Table 1. Details of the chosen test cases

Case	P_{back}(KPa)	$\overline{Kn}_0$ ($\times10^3$)	Re_t
1	---	8.01/9.67	406
2	7	3.24/6.92	260
3	15	1.95/1.63	269
4	25	1.93/1.13	257
5	35	1.01/0.914	247

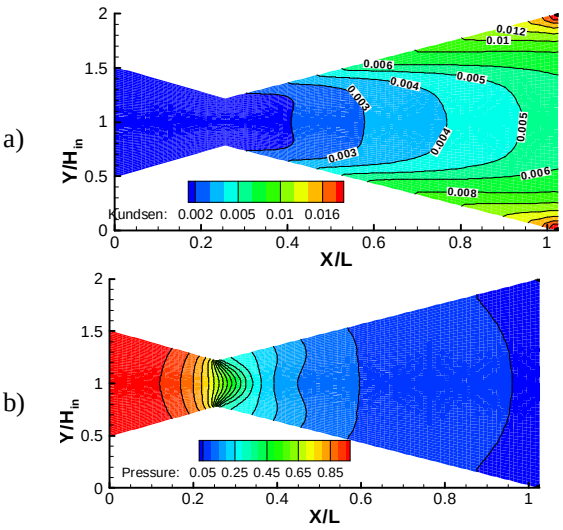

Figure 7. Knudsen number and pressure maps, Case 1

3.2 Supersonic flow

Figure 7-(a) shows Knudsen number contours for Case 1. The flow field obtained for this case is typical for supersonic micronozzles. The gas experience one order of magnitude rarefaction as the flow expands in the divergent section. The rarefaction is slightly stronger near the wall since wall heat transfer decreases the density more. In the vicinity of the nozzle lip, the impact of flow rarefaction is again significant. Figure 7-(b) shows the pressure contours. It is observed that pressure is non-uniform along the y-direction, i.e., dp/dy>0 in the convergent section and dp/dy<0 in the divergent section. Non-uniform pressure had already been observed for rarefied Poiseuille flow [20].

3.3 Effects of back pressure

3.3.1 Role of Boundary Layer

In this section, we study the effects of back pressure on the micronozzle behavior. Figure 8(a-d) shows the nozzle Mach contours when back pressure decreases from 35 to 7KPa. For all cases, flow chokes at the nozzle throat. In the divergent section, core regions of high Mach number are observed. The number of these Mach cores increases with the decrease of back pressure while the strength of them decays as flow approaches the outlet. Since the pressure at the exit region of nozzle is not uniform, it is mandatory to apply the back pressure at the end of an extended buffer zone. As the back pressure decreases, the first core moves away from the throat. It is observed that separated flow exists in considerable portion of the divergent section. The height of unseparated section is approximately equal for three first cases. Therefore, the flow passes through a conduit with approximately constant height in frames (a-c) rather than passing through a divergent section. This causes an overall reduced Mach number at the nozzle exit and decreased thrust production. The Mach contours in case (d) are similar to full supersonic case, see Fig. 4, expect near the outlet. Xu and Zhao [12] studied shock waves in very low Knudsen number micronozzle flows subject to back pressure. In comparison with their results, we observe that Mach cores are farther from the walls. This is due to stronger influence of viscosity/rarefaction in high Knudsen number flows studied here. Core regions are disappeared by a series of oblique/bow shocks. The strength of viscosity does not permit the shocks to approach the wall; therefore, closed regions of high Mach number appears. Figure 9 shows distribution of centerline Mach number under vacuum and different back-pressure conditions, i.e., 15, 25, and 35 KPa. As shown in this figure, the first bow shocks bring the Mach number slightly below unity. Then, the flow experiences a series of expansion/compressions along the nozzle.

3.3.2 Inviscid walls

In DSMC, viscosity is simulated via intermolecular and gas-wall collisions. To study the effects of wall boundary layer on the shock waves structures, we consider the gas-wall interactions as specular. Figure 10 shows Mach number contours for the same back pressures that was shown in Fig. 8 but for specular walls, i.e., the normal velocity component of incident particles is being reversed while the tangential component remains unchanged. Frame (a) shows that slight bow shocks appears just after the throat. The shock is normal to the walls and to the flow direction. Flow is subsonic in the rest of the nozzle. Again, the separation region near the wall is observed. This is due to the fact that the core flow is viscous. If we decrease the back pressure, shock moves closer to the outlet and separation region decreases. Once back pressure decreases to 7 KPa, the shock moves outside the nozzle and becomes oblique. Figure 11 shows distribution of Mach number along the centerline. Comparing this figure with Fig. 9, we can conclude that the appearance of expansion-compression waves is due to wall viscosity.

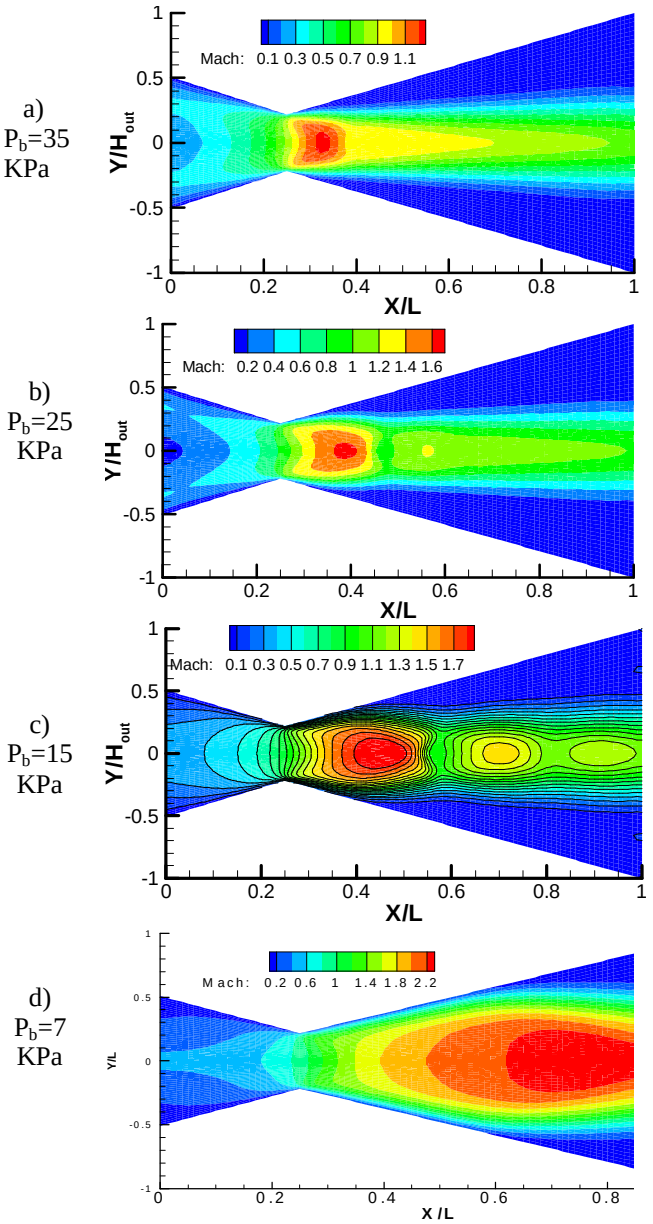

Figure 8 Mach number maps for different back pressures, viscous flow.

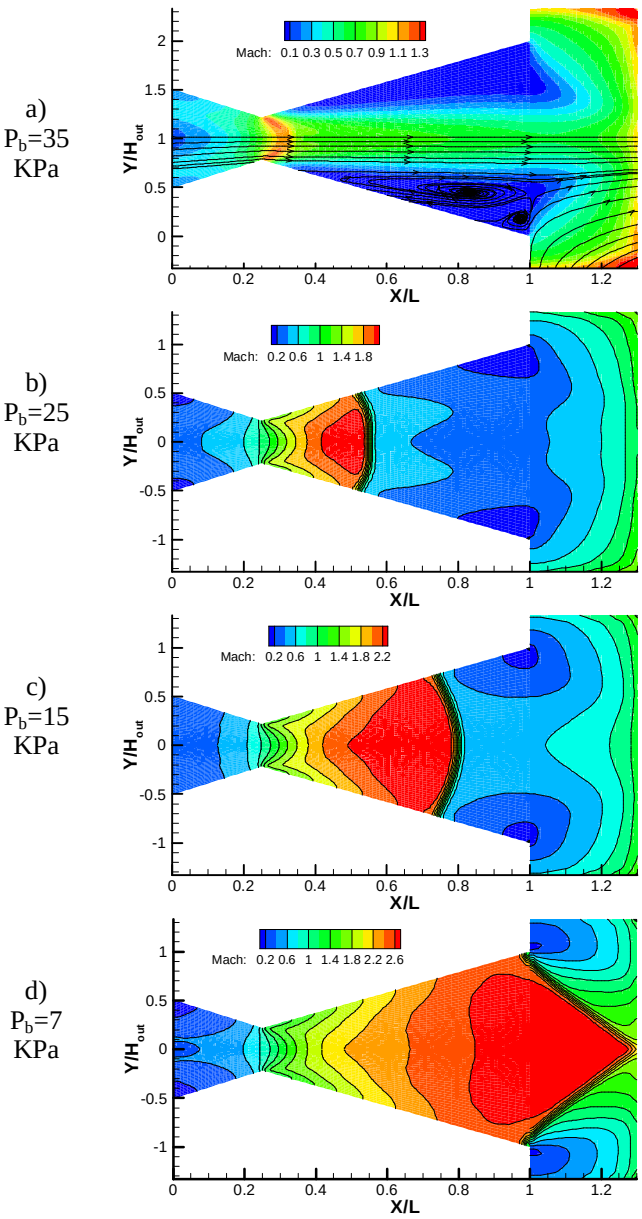

Figure 10 Mach number maps for different back pressures, inviscid flow.

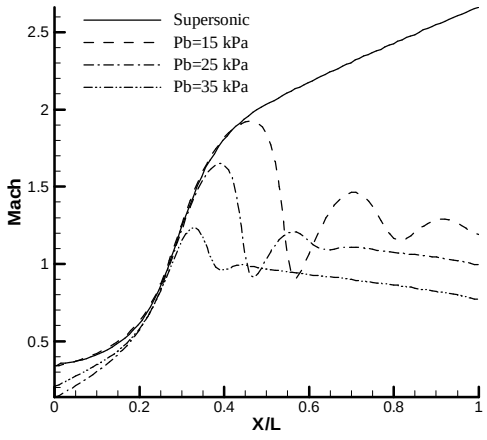

Figure 9. Mach number distribution along the centerline, viscous flow.

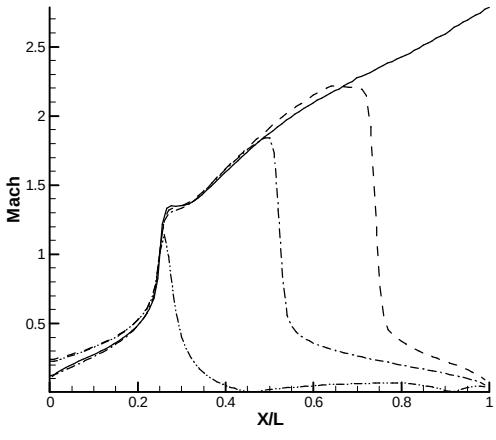

Figure 11. Mach number distribution along the centerline, inviscid flow.

3.3.3 Temperature Profiles

Figure 12 shows temperature profiles at different cross section along the viscous micronozzle for studied back pressures. Frame (a) refers to temperature profile in convergent section of the nozzle; therefore, there is slight decrease of temperature for all cases. Mixed effects of rarefaction, thermal boundary layer separation, and rapid conversion of the internal energy to kinetic one makes the temperature profile behaves in a complicated manner in divergent section.

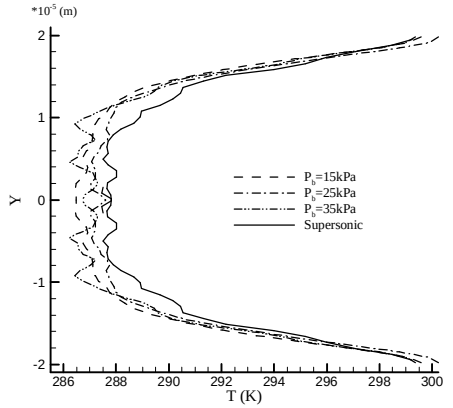

a) X/L=0.2

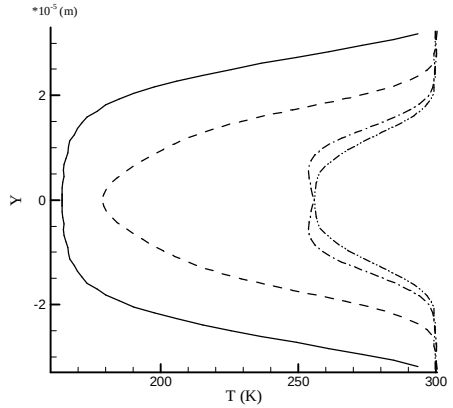

b) X/L=0.4

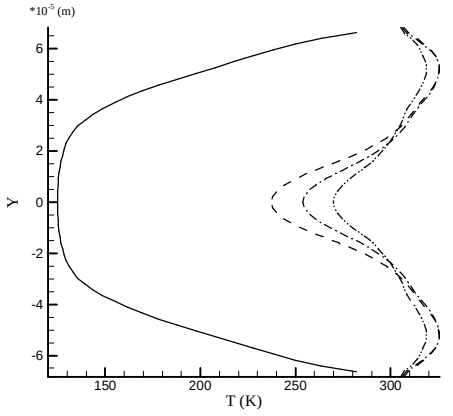

c) X/L=1

Figure 12. Temperature profiles at different back pressures

For supersonic flow, temperature decelerates along the nozzle. In frame (b), strong decrease in temperature is observed for P_{back}=15 KPa, which is due to occurrence of Mach core around X/L=0.4. The case with P_{back}=25 KPa shows slight heating at the centerline due to flow expansion. Temperature is constant in separated region in this frame but it increase in frame (c) as the flow exhausts to the environment. The decrease in temperature is stronger for lower back pressures, which is due to occurrence of stronger expansions in them.

3.4 Effects of Knudsen number

Our literature survey demonstrates that the past references [6-12] have not investigated the physics of high Knudsen number flows in micronozzles. Figure 13 shows contours of Mach number, for the same geometry previously considered but we increased the inlet Knudsen number to Kn_{in}=0.025. The average outlet Knudsen number is Kn_{out}=0.521 for frame (a), Kn_{out}=0.382 for frame (b), and Kn_{out}=0.244 for frame (c). Frame (a) shows unique behavior, i.e., subsonic flow does not choke at the throat but accelerates in the divergent section. Mach number reaches a value of unity at the exit of buffer zone. The acceleration of subsonic flow in the divergent section is quit unexpected. In fact, it is impossible to establish supersonic flow at this high inlet Knudsen number condition. As the viscose force dominates the flow with the increase of Knudsen number, the dissipation of kinetic energy is so high that flow neither chokes at the throat nor accelerates to supersonic condition in the divergent section. To confirm the role of viscosity, we simulated the same case with inviscid wall conditions; see Fig. 13-(b). It is observed that flow chokes and accelerate in divergent section. A series of bow shocks appear which only decrease the supersonic flow to lower supersonic state.

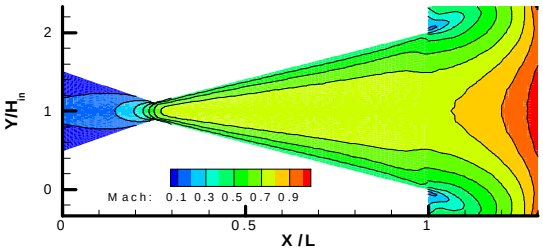

a) Supersonic outlet, viscous

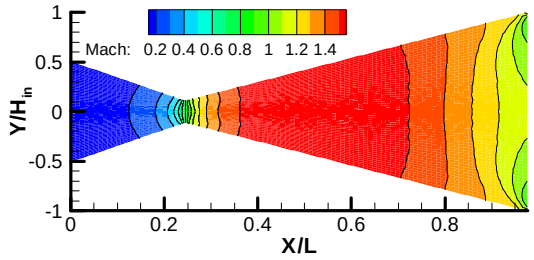

b) Supersonic outlet, inviscid

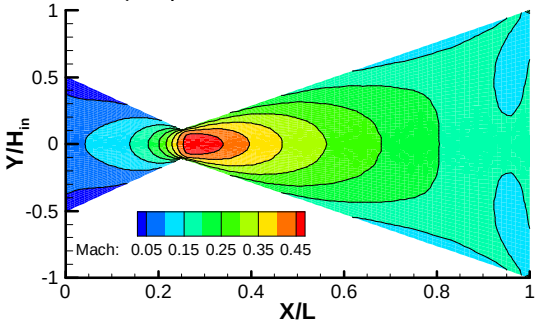

c) Subsonic outlet, viscous, P_{back}=20 kPa

Figure 13. Mach number contours, Kn_{in}=0.025.

Figure 13-(c) shows Mach contours for the case with a back pressure of 20 KPa. Flow reaches a maximum Mach number of 0.45 at the throat and does not choke. Subsonic flow decelerates in the divergent section, which is quit physical behavior for subsonic flow. Therefore, we conclude that thick viscous boundary layers prevent the formation of supersonic flow at higher inlet Knudsen numbers in divergent section of micronozzles. The physics implies that flow must be subsonic in the nozzle and this requires applying a back pressure at the end of nozzle. It should be noted that similar results are observed for higher inlet Knudsen number flows.

4. Conclusion

Supersonic and subsonic flows in micro convergent-divergent nozzles were simulated using an unstructured DSMC solver. The mixed impacts of rarefaction, compressibility, and viscous forces were clearly observed in determining the flow behavior in the micronozzle. The use of a buffer zone far from the nozzle exit allows one to eliminate the possible impact of non-uniform pressure at the nozzle exit. If we apply a back pressure at the outlet, high viscous force prevents the formation of normal shocks; instead, regions of high Mach appear which diminish due to formation of bow shocks. In this case, the flow passes through an approximately constant height conduit rather than a divergent nozzle because a significant portion of the flow separates near the wall. If we eliminate the viscosity of walls, we observe that thick bow shocks appear which are normal to the walls. Meanwhile, separated region still exists as the main flow is viscous. We observed that it is impossible to set up supersonic flow in micronozzles as soon as the inlet Knudsen number exceeds a moderate level. This phenomenon is due to strong viscous force. Alternatively, to obtain physical solution, it is required to apply a back pressure at the outlet so that physical subsonic flow is captured inside the micronozzle.

Acknowledgment

The authors would like to thank the Graduate Study Office of Sharif University of Technology for financial supports.

References

1. Bird, G. A., 1994, Molecular Gas Dynamics and the Direct Simulation of Gas Flows, Clarendon, Oxford.
2. Fang, Y., Liou, W.W., 2002, Computations of the Flow and Heat Transfer in Microdevices Using DSMC with Implicit Boundary Conditions, Journal of Heat Transfer, Vol. 124, 338-345.
3. Wang, M., and Li, Z., 2004, Simulations for gas flows in microgeometries using the Direct Simulation Monte Carlo Method, International Journal of Heat & Fluid Flow, Vol. 25, pp. 975–985.
4. Roohi, E., Darbandi, M., Mirjalili, V., DSMC solution of supersonic scale to choked subsonic flow in micro to nano channels, ICNMM2008-62282, Proceedings of the 6th Int. ASME Conference on Nanochannels, Microchannels and Minichannels, Germany, 2008.
5. Roohi, E., Darbandi, M., Mirjalili, V., DSMC solution of subsonic flow through micro-nano scale channels, Journal of Heat Transfer, accepted.
6. Alexeenko, A.A., Levin, D.A., Gimelshein, S.F., Collins, R.J., Reed, B.D., 2002, Numerical modeling of axisymmetric and three-dimensional flows in microelectromechanical systems nozzles, AIAA Journal, 40 (5), 897–904.
7. Louisos, W.F., Hitt, D.L. (2005) Optimal Expander Angle for Viscous Supersonic Flow in 2d Micro-nozzles, AIAA Paper 2005-5032.
8. Alexeenko A., Fedosov, D. A., Gimelshein S. F., Levin D. A., Collins, R. J., 2006, Transient Heat Transfer and Gas Flow in a MEMS-Based Thruster, Journal of Microelectromechanical Systems, Vol. 15 (1). pp. 181-194.
9. Liu, M., Zhang, X., Zhang, G. and Chen Y., 2006, "Study on micronozzle flow and propulsion performance using DSMC and continuum methods", Acta Mechanica Sinica, Vol. 22, pp. 409-416.
10. Xie, C., 2007, Characteristics of micronozzle gas flows, Physics of Fluids, Vol. 19, 037102.
11. Titove, E. V., Levin, D. A., 2007, Extension of DSMC method to high pressure flows, International Journal of Computational Fluid Dynamics, Vol. **21** (9-10), pp. 351-368.
12. Xu, J., Zhao, C., Two-dimensional numerical simulations of shock waves in micro convergent–divergent nozzles, International Journal of Heat and Mass Transfer 50 (2007) 2434–2438.
13. Louisos, W.F., Alexeenko, A.A., Hitt, D.L., Zilić, A. (2008), Design considerations for supersonic micronozzles, Int. J. Manufacturing Research, Vol. 3 (1), pp. 80–113.
14. Zhou, Q., Leschziner, M.A., 1999, An improved particle-locating algorithm for Eulerian–Lagrangian computations of two-phase flows in general coordinates, International Journal of Multiphase Flow, 25, 813–825.
15. Chen, X. Q., Pereira, J.C.F., 1999, A new particle-locating method accounting for source distribution and particle-field interpolation for hybrid modeling of strongly coupled two-phase flows in arbitrary coordinates, Numerical Heat Transfer, Part B 35, 41–63.
16. Macpherson, G. B., Nordin, N., Weller, H. G., Particle tracking in unstructured, arbitrary polyhedral meshes for use in CFD and molecular dynamics, Communications in Numerical Methods in Engineering, 2008.
17. Darbandi, M., and Vakilipour, S., 2007, Developing Consistent Inlet Boundary Conditions to Study the Entrance Zone in Microchannels., Journal of Thermophysics and Heat Transfer, Vol. **21** (3) , pp. 596-607.
18. Vakilipour, S., Darbandi, M., 2009, Advancement in numerical study of gas flow and heat transfer in microchannels, Journal of Thermophysics and Heat Transfer, Vol. **23** (1), pp. 205-208.
19. Darbandi, M., Vakilipour, S., Solution of Thermally Developing Zone in Short Micro/Nano Scale Channels, Journal of Heat Transfer, in Press, (March 2009).
20. Uribe, F.J., Garcia, A. L., Burnett Description for Plane Poiseuille Flow, Physical Review E, 60(4), (1999), 4063-4078.